Chemical Geology, 53 (1985) 109—124
Elsevier Science Publishers B.V., Amsterdam — Printed in The Netherlands

THE KINETICS OF CALCITE DISSOLUTION AND PRECIPITATION IN GEOLOGICALLY RELEVANT SITUATIONS OF KARST AREAS
2. Closed System

DIETER BUHMANN and WOLFGANG DREYBRODT*

Fachbereich 1, Physik, Universität Bremen, 2800 Bremen 33 (Federal Republic of Germany)

(Received August 10, 1984; revised and accepted February 18, 1985)

Abstract

Buhmann, D. and Dreybrodt, W., 1985. The kinetics of calcite dissolution and precipitation in geologically relevant situations of karst areas, 2. Closed system. Chem. Geol., 53: 109—124.

A general theory of dissolution and precipitation rates of calcite in the pure $CaCO_3$—CO_2—H_2O system under closed-system conditions is presented. The three rate-limiting processes, surface-controlled dissolution or precipitation at the $CaCO_3$ surface, diffusion of the molecular and ionic species, and slow conversion of CO_2 into HCO_3^- are treated simultaneously. Dissolution and precipitation rates are calculated as a function of the Ca^{2+} concentration in the solution at various temperatures T and partial pressures of CO_2, P_{CO_2}, in the solution. The rates can in all cases be approximated by a linear dependence $R = \alpha([Ca^{2+}]_{eq} - [Ca^{2+}])$, where $\alpha = \alpha(T, P_{CO_2}, \delta)$ and 2δ is the thickness of the water film enclosed by two calcite surfaces. Values of α are summarized in two tables which provide the geologist with data from which dissolution rates of pure limestone can be derived easily. The calculated rates for turbulent flow are one order of magnitude higher than those for laminar flow. This provides the first theoretical explanation of the so-called hydraulic jump.

We have carried out dissolution experiments to determine the time dependence of the Ca^{2+} concentration in stagnant and turbulently stirred H_2O films at given P_{CO_2}, δ and T. From the time constants of the exponential behaviour of $[Ca^{2+}](t)$ the values of α have been determined. They are in good agreement with the theory.

1. Introduction

The development of karstification in limestone areas is mainly determined by dissolution processes in the $CaCO_3$—CO_2—H_2O system. Knowledge of the equilibrium chemistry of the system does not suffice to understand these processes but one has also to know the kinetics of the dissolution process, from which the dissolution rates can be derived. In a recent paper (Buhmann and Dreybrodt, 1985) we have developed a theory of dissolution and precipitation rates of calcite for the case of open systems. We have regarded water films of various thicknesses flowing on calcite surfaces under laminar or turbulent flow, with a free surface open to an atmosphere containing CO_2. CO_2 exchange over this surface

*Author to whom all correspondence should be sent.

0009-2541/85/$03.30

is possible during dissolution or precipitation of calcite. Although this situation is relevant in many processes of karstification in the vadose and unsaturated zone, where freely flowing water is present, the most important processes of karstification take place in the phreatic zone under closed-system conditions. In this case the water flows in completely filled conduits and exchange of CO_2 is not possible, since no free surface to the atmosphere exists.

In the following text, by using the general principles of our theory recently developed for the case of the open system, and by modifying the boundary conditions, we present a general theory of dissolution and precipitation of $CaCO_3$ in the closed system.

The kinetics of calcite dissolution and precipitation is determined by three independent processes:

(a) The kinetics of dissolution at the phase boundary between the solvent aqueous system $CaCO_3$—H_2O—CO_2 and the solid $CaCO_3$.

(b) The kinetics of the conversion of dissolved CO_2 to $H_2CO_3^0$ which constitutes the aggressive agent in the process of $CaCO_3$ dissolution.

(c) Mass transport of the dissolved species, i.e. Ca^{2+}, CO_3^{2-}, HCO_3^- and CO_2^0 by diffusion from and to the phase boundaries.

The first process has been investigated in detail by Plummer et al. (1978, 1979) who give a rate equation (PWP equation) from which the flow of Ca^{2+} can be calculated if the activities of Ca^{2+}, HCO_3^-, H_2CO_3 and H^+ at the phase boundary are known.

The mechanisms determining conversion of CO_2 to $H_2CO_3^0$, which is a slow process, have recently been reviewed by Usdowski (1982) and formerly by Kern (1960). A first approach to calculating dissolution rates for closed systems by considering the PWP rate equation and conversion of CO_2 to $H_2CO_3^0$ has been given by Dreybrodt (1981a, b). This theory applies well to all cases where mass transport by diffusion plays the minor part in the processes listed above. This is the case for very thin water films flowing laminarly in narrow joints, a situation applying to the initial processes of karstification, and for all situations where the flow of water is turbulent. The application of his results yielded good understanding of the processes of karst initiation as well as the development in mature karst systems, where dissolution proceeds under turbulent flow.

In contrast to the case of dissolution in open systems, some experimental data were available for closed-system conditions. Howard and Howard (1967) measured dissolution rates on natural limestones in artificial joint openings, through which water was forced in laminar flow. Rauch and White (1977) obtained dissolution rates under conditions of turbulent flow. Although the experimental conditions were not quite that of the theory the agreement with the theoretical predictions of Dreybrodt (1981a) was remarkable and encouraging.

We have now developed a theory which is applicable also in the region where mass transport by diffusion plays the dominant role, and carried out experiments under more adequate conditions to verify the theoretical predictions.

2. Theory of calcite dissolution

2.1. Formulation of the problem

Closed-system conditions are widespread in natural surroundings. Waters percolating downwards through narrow joints in the vadose zone or water conduits in the phreatic zone are examples. Joint widths range from roughly 10^{-3} cm to a few centimeters. The dimensions of conduit diameters in the phreatic zone vary from a few millimeters up to 10 m. Water flow is laminar in most cases when the dimensions of joints or conduits are below 0.1 cm. At dimensions larger than 0.5 cm usually turbulent flow sets in. To obtain equations which are mathematically treatable, we have to idealize the variety of shapes existing in conduits. We do this by assuming that all conduits are bounded by two parallel planes

separated by distance 2δ. This introduces errors by geometrical factors, which are in the order of magnitude of one and do not play an important role in the application to real geological problems, where the knowledge of rates within one order of magnitude is sufficient.

A further simplification is introduced by neglecting the velocity distribution perpendicular to the flow direction in both laminar and turbulent flow, i.e. assuming plug flow. This also has no serious influence on the order of magnitude (Dreybrodt, 1981a). We have shown in our recent paper that with these assumptions, the equations of mass transport for the stationary state in plug flow are determined only by the contact time of the solution to the rock and are equivalent to the equations of mass transport in stagnant films, describing the time development of the dissolved species (Buhmann and Dreybrodt, 1985). This is a very important fact, since it permits design of simple experiments, which are equivalent to the conditions of flowing solutions.

With these approximations we are able to formulate the problem mathematically. Fig. 1

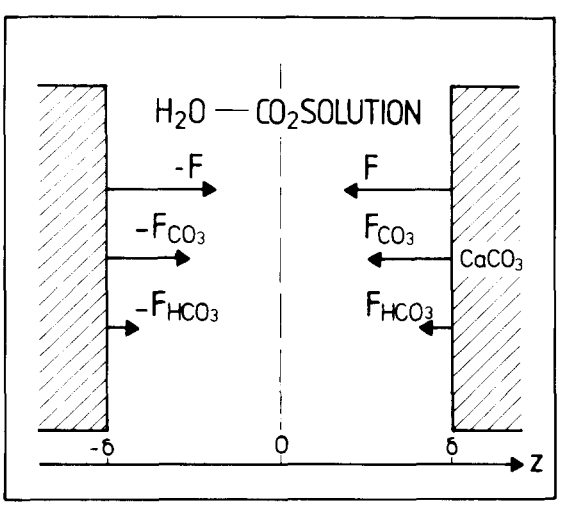

Fig. 1. Geometrical model of the $CaCO_3$ dissolution in a system closed to the atmosphere.

shows the geometric situation. A water film of thickness 2δ is enclosed by two parallel plates of $CaCO_3$ in the x—y-plane. No CO_2 can enter or leave the system. The geometry is symmetric with respect to $z = 0$ and it suffices to find solutions in the region $0 \leqslant z \leqslant \delta$, since the symmetry of the problem implies that the concentration profiles of all species are even functions in z and are continuous. Therefore, the first derivatives at $z = 0$ are all zero and no flux of any species is possible at $z = 0$. At $z = \pm\delta$ a flux of Ca^{2+}, CO_3^{2-} and HCO_3^- is directed into the bulk of the solution.

Dissolution stoichiometry requires that for each Ca^{2+} dissolved from the $CaCO_3$ surface one molecule of CO_2 has to be converted into $H_2CO_3^0$, which delivers a H^+ ion to remove the accompanying CO_3^{2-} ion by conversion into the soluble HCO_3^- ion.

The flux of Ca^{2+} ions is given by the equation of Plummer et al. (1978) (PWP equation):

$$F = \kappa_1(H^+)_\delta + \kappa_2(H_2CO_3^*)_\delta + \kappa_3 - \kappa_4(Ca^{2+})_\delta\,(HCO_3^-)_\delta \qquad (1)$$

The round brackets relate to the activities of the corresponding species, the subscript δ indicates the activities at the solution–calcite boundary at $z = \delta$, and:

$$(H_2CO_3^*) = (H_2CO_3^0) + (CO_2)_{aq}$$

The κ_i are rate constants and their temperature dependence has been taken from Plummer et al. (1978). In addition κ_4 depends on the concentration of $H_2CO_3^0$.

We now outline our theory for open systems (Buhmann and Dreybrodt, 1985), and give therefore only a short summary of the equations needed to calculate the case of closed systems. These equations provide a general model including the three possible rate-limiting processes (a), (b) and (c) considered above.

The mass transport of CO_2, HCO_3^-, CO_3^{2-} and Ca^{2+} towards and away from the boundaries is given by:

$$-\frac{\partial[CO_2]}{\partial t} + D_{CO_2}\frac{\partial^2[CO_2]}{\partial z^2} = (k_1 + k_2[OH^-]) \times [CO_2] - (k_{-1}[H^+] + k_{-2})[HCO_3^-] = R_{CO_2} \quad (2a)$$

$$-\frac{\partial[HCO_3^-]}{\partial t} + D\frac{\partial^2[HCO_3^-]}{\partial z^2} = -(k_1 + k_2[OH^-])[CO_2] + (k_{-1}[H^+] + k_{-2})[HCO_3^-] + k_{-3}[H^+][CO_3^{2-}] - k_3[HCO_3^-] \quad (2b)$$

$$-\frac{\partial[CO_3^{2-}]}{\partial t} + D\frac{\partial^2[CO_3^{2-}]}{\partial z^2} = k_3[HCO_3^-] - k_{-3}[H^+][CO_3^{2-}] \quad (2c)$$

$$-\frac{\partial[Ca^{2+}]}{\partial t} + D\frac{\partial^2[Ca^{2+}]}{\partial z^2} = 0 \quad (2d)$$

The square brackets denote concentrations. D_{CO_2} and D are the molecular diffusion coefficients in the case of laminar flow. In the case of turbulent flow they have to be replaced by eddy diffusivities D_e, which are higher by about a factor of 10^4 than the molecular diffusion coefficients (Skelland, 1974).

The right-hand side of the equations describes the conversion of:

$$CO_2 \rightleftharpoons H_2CO_3^0 \rightleftharpoons HCO_3^- \rightleftharpoons CO_3^{2-}$$

The conversion of CO_2 to HCO_3^- is a slow process and is described by the reaction rate constants k_1, k_{-1} and k_2, k_{-2}, which respectively represent two different chemical pathways:

$$CO_2 + H_2O \underset{k_{-1}}{\overset{k_1}{\rightleftharpoons}} H^+ + HCO_3^-$$

$$CO_2 + OH^- \underset{k_{-2}}{\overset{k_2}{\rightleftharpoons}} HCO_3^-$$

The fast process $H_2CO_3^0 \rightleftharpoons HCO_3^-$ has been omitted here. The rate constants k_3, k_{-3} describe conversion of $HCO_3^- \rightleftharpoons H^+ + CO_3^{2-}$, which is a fast process too and is introduced for completeness. Since conversion of CO_2 is the only slow process, we can assume that the only species not in equilibrium with each other are CO_2 and HCO_3^-, CO_2 and CO_3^{2-}, and CO_2 and $H_2CO_3^0$, since $H_2CO_3^0$ is converted by a fast process into $HCO_3^- + H^+$ and is therefore in equilibrium with HCO_3^-. Thus, eqs. 2a and 2b represent a coupled nonlinear system. Eq. 2d is independent of the others, since no reaction of Ca^{2+} with other species occurs if one neglects ion pairing. If ion pairing is included one obtains an analogous system of equations where in eq. 2d $[Ca^{2+}]$ is replaced by:

$$[Ca^{2+}]_T = [Ca^{2+}] + [CaCO_3^0] + [CaHCO_3^+]$$

Since during dissolution all the species H^+, OH^-, $H_2CO_3^0$, HCO_3^- and CO_3^{2-} are in equilibrium with each other, we need the mass-balance equations to describe their mutual dependence. They are:

$$(H^+)(OH^-) = K_w(H_2O) \quad (3a)$$

$$(CO_2) = K_H P_{CO_2} \quad (3b)$$

$$(CO_2) = K_0(H_2CO_3^0) \quad (3c)$$

$$(H^+)(HCO_3^-) = K_1(H_2CO_3^*) \quad (3d)$$

$$(H^+)(CO_3^{2-}) = K_2(HCO_3^-) \quad (3e)$$

$$(Ca^{2+})(HCO_3^-) = K_3(CaHCO_3^+) \quad (3f)$$

$$(Ca^{2+})(CO_3^{2-}) = K_4(CaCO_3^0) \quad (3g)$$

$$(H^+)(HCO_3^-) = K_5(H_2CO_3^0) \quad (3h)$$

$$(H^+)(HCO_3^-) = K_6(CO_2)(H_2O) \quad (3i)$$

A survey of the temperature dependence of the equilibrium constants, the rate constants, and molecular diffusion coefficients used in this work is given in table I of our recent paper (Buhmann and Dreybrodt, 1985).

2.2. Calculation of the dissolution rates

To solve the coupled differential equations

(2), we start with eq. 2d, which is independent of the others. The boundary conditions for the Ca^{2+} species are:

$$-D \left.\frac{\partial[Ca^{2+}]}{\partial z}\right|_{z=\delta} = F([H^+]_\delta, [HCO_3^-]_\delta, [Ca^{2+}]_\delta)$$
$$-D \left.\frac{\partial[Ca^{2+}]}{\partial z}\right|_{z=0} = 0 \qquad (4)$$

The flux F is given by the PWP equation (1) and depends on the chemical composition of the solution at the solid—liquid interface, which is determined by the mass transport and the chemical reactions which govern eqs. 2a—2c. If we assume that the dissolution proceeds slowly, that during the time which is needed to build up a stationary profile of $[Ca^{2+}]$ across the water film the composition of the solution remains constant, we have also the situation that F remains practically constant. In this case the solution of eq. 2d with boundary conditions (4) is given by Carslaw and Jaeger (1959):

$$[Ca^{2+}](z) = \frac{Ft}{\delta} + \frac{F\delta}{D}\left(\frac{3z^2-\delta^2}{6\delta^2}\right) - \frac{F\delta}{3D} + [Ca^{2+}]_\delta \qquad (5)$$

$[Ca^{2+}]_\delta$ is the Ca^{2+} concentration at time $t = 0$. The time which is needed to build up a stationary profile is:

$$t_D = \delta^2/D\pi^2$$

and our approximation holds as long as $t_D \ll \tau$, where τ is the exponential decay time of the solution to reach saturation. In the case of laminar flow this is realized for values of $\delta \leqslant 0.3$ cm. In the case of turbulent flow t_D becomes smaller by a factor of at least $\sim 10^4$ and the concentration profiles build up immediately even in the case of large δ in the order of several meters (Skelland, 1974).

To solve the coupled eqs. 2a—2c we use a method proposed by Quinn and Otto (1971). Adding eqs. 2a—2c leads to:

$$\frac{\partial[CO_2]}{\partial t} + \frac{\partial[HCO_3^-]}{\partial t} + \frac{\partial[CO_3^{2-}]}{\partial t} = D_{CO_2}\frac{\partial^2[CO_2]}{\partial z^2} + D\frac{\partial^2[HCO_3^-]}{\partial z^2} + D\frac{\partial^2[CO_3^{2-}]}{\partial z^2} \qquad (6)$$

The left-hand side of this equation represents the increase of total carbon in the solution. The concentration of the missing species $H_2CO_3^0$ is small compared to those of the other carbon-containing species and can therefore be neglected. Since each dissolved Ca^{2+} ion releases also one C atom, we have by using eq. 5:

$$\frac{\partial[CO_2]}{\partial t} + \frac{\partial[HCO_3^-]}{\partial t} + \frac{\partial[CO_3^{2-}]}{\partial t} = \frac{\partial[Ca^{2+}]}{\partial t} = F/\delta \qquad (7)$$

Integrating eq. 6 yields then:

$$\frac{F}{\delta}z + C_1 = D_{CO_2}\frac{\partial[CO_2]}{\partial z} + D\frac{\partial[HCO_3^-]}{\partial z} + D\frac{\partial[CO_3^{2-}]}{\partial z} \qquad (8)$$

The integration constant C_1 is determined from the boundary conditions at $z = 0$ and turns out to be $C_1 = 0$. After second integration we obtain:

$$\frac{F}{2\delta}z^2 + C_2 = D_{CO_2}[CO_2] + D[HCO_3^-] + D[CO_3^{2-}] \qquad (9)$$

C_2 is derived from the boundary conditions at $z = \delta$:

$$C_2 = -\tfrac{1}{2}F\delta + D_{CO_2}[CO_2]_\delta + D[HCO_3^-]_\delta + D[CO_3^{2-}]_\delta \qquad (10)$$

Using the mass action equations (3) and the condition of electroneutrality it is possible

to express all the quantities on the right-hand side of eq. 2a, i.e. $[HCO_3^-]$, $[H^+]$ and $[OH^-]$ as a function of $[CO_2]$ and $[Ca^{2+}](z)$. Thus eq. 2a is decoupled and can be solved numerically.

The equation of electroneutrality, neglecting ion pairs, reads:

$$2[Ca^{2+}] + [H^+] = [HCO_3^-] + [OH^-] + 2[CO_3^{2-}] \quad (11)$$

Inserting the mass action equations (3a) and (3e) for $[CO_3^{2-}]$ and $[OH^-]$ into eq. 11 yields a quadratic equation with the solution:

$$[H^+] = -\tfrac{1}{2}(2[Ca^{2+}] - [HCO_3^-]) + \left\{ \frac{(2[Ca^{2+}] - [HCO_3^-])^2}{4} + \frac{K_w}{\gamma_H \gamma_{OH}} + \frac{2K_2 \gamma_{HCO_3}}{\gamma_H \gamma_{CO_3}} [HCO_3^-] \right\}^{1/2} \quad (12)$$

The γ_i's are the activity coefficients and are calculated by modified Debye—Hückel theory. The ionic strength has been taken as independent of z by using the approximation:

$$I = 3[Ca^{2+}]_{av}$$

where $[Ca^{2+}]_{av}$ is the averaged concentration from $z = 0$ to $z = \delta$.

The concentration of CO_3^{2-} can be calculated from eq. 12 by inserting into the corresponding mass action equation (3e). Finally, inserting this and eq. 12 into eq. 9 yields a cubic relation for $[HCO_3^-]$ as a function of $[Ca^{2+}](z)$, $[CO_2]$ and z only:

$$L[HCO_3^-]^3 + M[HCO_3^-]^2 + N[HCO_3^-] + P = 0 \quad (13)$$

with

$$L = K_2 \frac{\gamma_{HCO_3}}{\gamma_H \gamma_{CO_3}}$$

$$M = \frac{K_w}{\gamma_H \gamma_{OH}} - L^2 + 3BL + 2L[Ca^{2+}](z)$$

$$N = 2B\left(\frac{K_w}{\gamma_H \gamma_{OH}} + L[Ca^{2+}](z) + BL\right)$$

$$P = B^2 \frac{K_w}{\gamma_H \gamma_{OH}}$$

$$B = D^{-1}(-\tfrac{1}{2} F \delta^{-1} z^2 + \tfrac{1}{2} F\delta - D_{CO_2}([CO_2]_\delta - [CO_2](z)) - D([HCO_3^-]_\delta + [CO_3^{2-}]_\delta))$$

Including ion pairs yields a somewhat more complicated third-order expression, where $[Ca^{2+}](z)$ is replaced by $[Ca^{2+}]_T(z)$. Our calculations have shown that introduction of ion pairing changes the results by less than 3%. Therefore, ion pairs can be neglected without loss of the general validity of our theory.

Inserting the solution of eq. 13, eq. 12 and the mass action equation (3a) into eq. 2a yields a differential equation for $[CO_2]$ which depends only on z, $[Ca^{2+}]_\delta$, $[HCO_3^-]_\delta$ and $[CO_2]_\delta$. Its correct solution has to satisfy the condition of stoichiometry, i.e. for each dissolved Ca^{2+} ion one CO_2 molecule has to be converted into $H_2CO_3^0$. Thus:

$$F([Ca^{2+}]_\delta, [HCO_3^-]_\delta) = -\int_0^\delta R_{CO_2} \, dz \quad (14)$$

R_{CO_2} is the conversion rate of CO_2 and is given by the right-hand side of eq. 2a. The boundary conditions for $[CO_2]$ are:

$$\partial[CO_2]/\partial z = 0$$

for

$$z = 0 \quad \text{and} \quad z = \delta$$

since at $z = \delta$ no direct reaction of CO_2 with $CaCO_3$ occurs.

With these conditions eq. 2a is solved numerically by a Runge—Kutta procedure (Kamke, 1967). We choose values of $[CO_2]_\delta$ and $[Ca^{2+}]_\delta$, and a realistic value of $[HCO_3^-]_\delta$ close to $2[Ca^{2+}]_\delta$. From this, $[H^+]_\delta$ and $[H_2CO_3^*]_\delta$ in equilibrium with $[H^+]_\delta$ and

$[HCO_3^-]_\delta$ are calculated. Inserting these values into the PWP equation (1) yields the flux F of Ca^{2+} at $z = \delta$. Now $[Ca^{2+}](z)$ can be computed. In the next step we start the Runge—Kutta procedure with a chosen value $[CO_2]_\delta$. To achieve the correct solution, $[HCO_3^-]_\delta$ is changed in a half-step procedure until eq. 14 holds to an accuracy of 1%. From the values thus obtained we calculate the initial CO_2 concentration $[CO_2]_i$. $[CO_2]_i$ is the CO_2 concentration of the initial H_2O—CO_2 solvent, when no $CaCO_3$ has yet been dissolved. Then we change $[CO_2]_\delta$ until the calculated value $[CO_2]_i^{calc}$ differs by less than 1% from the stated value $[CO_2]_i$.

This procedure yields the concentration profiles of $[CO_2]$, $[HCO_3^-]$, $[H^+]$, $[CO_3^{2-}]$ and $[Ca^{2+}]$ as well as the correct dissolution rates $F([Ca^{2+}]_{av})$. Fig. 2 gives a simplified flow diagram of these calculations.

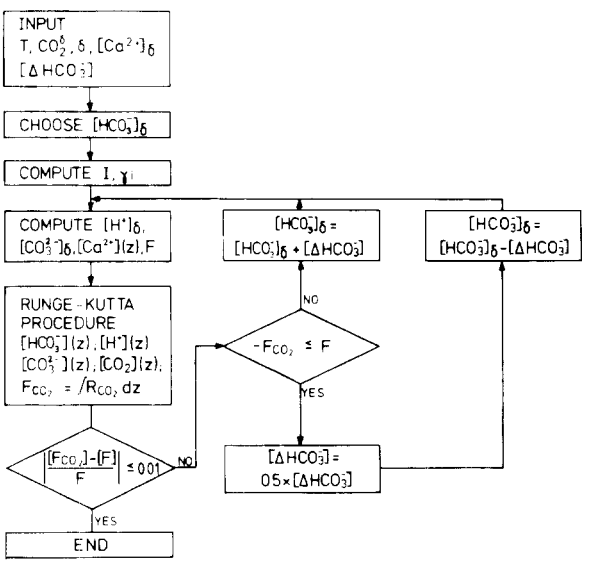

Fig. 2. Flow diagram for the numerical calculations.

The initial concentration $[CO_2]_i$ can be obtained by the following considerations. The initial concentrations in a solution in equilibrium with P_{CO_2} are:

$$[CO_3^{2-}]_i \cong 0 \tag{15a}$$

$$[Ca^{2+}]_i = 0 \tag{15b}$$

$$[HCO_3^-]_i = [H^+]_i \tag{15c}$$

$$[CO_2]_i = K_H P_{CO_2} \tag{15d}$$

$$[H_2CO_3^0]_i = [CO_2]_i / K_0 \tag{15e}$$

During the process of dissolution the sum of the average concentrations of all carbon-containing species must be equal to the sum of the corresponding initial concentrations augmented by the average concentration of Ca^{2+}. Thus we have:

$$[CO_2]_i + [H_2CO_3]_i + [HCO_3^-]_i + [Ca^{2+}]_{av} = [CO_2]_{av} + [H_2CO_3]_{av} + [HCO_3^-]_{av} + [CO_3^{2-}]_{av} \tag{16}$$

Using eq. 15 and the equations of mass action one obtains:

$$[CO_2]_i = \frac{S}{1 + 1/K_0} + \frac{K_6}{2\gamma_H \gamma_{HCO_3}(1 + 1/K_0)^2} - \frac{1}{2(1 + 1/K_0)} \left\{ \frac{K_6}{\gamma_H \gamma_{HCO_3}(1 + 1/K_0)} \times \left(4S + \frac{K_6}{\gamma_H \gamma_{HCO_3}(1 + 1/K_0)} \right) \right\}^{1/2}$$

with

$$S = [CO_2]_{av} + [H_2CO_3]_{av} + [HCO_3^-]_{av} + [CO_3^{2-}]_{av} - [Ca^{2+}]_{av} \tag{17}$$

The γ^i's are the initial activities of the corresponding ions and their values are ~ 1.

For all cases of interest, i.e. pH ⩽ 9 and $S \geqslant 10^{-4}$ mmol cm^{-3}, this can be approximated, with an error of less than 3%, by:

$$[CO_2]_i = \{[CO_2]_{av} + [Ca^{2+}]_{av}\} \tag{18}$$

As a final remark in this section we wish to stress that this theory is also applicable to the case of calcite precipitation. The only difference is that the signs of F and R_{CO_2} are reversed, since the flux of Ca^{2+} is directed towards the calcite surface and CO_2 is released

into the solution. In the calculations of precipitation in the closed system we start with a supersaturated solution with concentrations $[Ca^{2+}]_s$ and $[CO_2^0]_s$. The relation between $[CO_2]_{av}$ and $[Ca^{2+}]$ and $[CO_2]_s$ is now:

$$[CO_2]_{av} = [CO_2]_s + [Ca^{2+}]_{av} - [Ca^{2+}]_s \quad (19)$$

for all cases of interest.

2.3. Results

We have calculated the dissolution rates at temperatures $T = 5°$, $10°$ and $20°C$ for initial pressures $P^i_{CO_2}$ in the range of 0.01—0.1 atm. (Table I). This is the range of realistic P_{CO_2} pressures in the soil, where CO_2 equilibrates with the water percolating before it enters closed-system conditions.

Fig. 3 shows the results for $P_{CO_2} = 5 \cdot 10^{-2}$ atm. We have plotted the dissolution rates as functions of $[Ca^{2+}]_{av}$, which also represents the experimentally measured value of the Ca^{2+} concentration (cf. Section 3), and is obtained by averaging eq. 5 over the water film:

$$[Ca^{2+}]_{av} = [Ca^{2+}]_\delta - F\delta/3D \quad (20)$$

In all cases of laminar flow and in most cases of turbulent flow the curves can be approximated with sufficient accuracy at Ca^{2+} concentrations greater than $0.2[Ca^{2+}]_{eq}$ by a linear function:

$$F = \alpha\{[Ca^{2+}]_{eq} - [Ca^{2+}]_{av}\} \quad (21)$$

$[Ca^{2+}]_{eq}$ is the corresponding equilibrium concentration and is a function of δ, $P^i_{CO_2}$ and T. Numerical values of α are given in Table I.

At very low film thicknesses ($\delta \leqslant 0.002$ cm), α increases linearly with δ. This is the region where conversion of $CO_2 \rightarrow H_2CO_3^0$ is

TABLE I

Calculated values of α in 10^{-5} cm s^{-1} for various pressures of CO_2, temperatures and film thicknesses δ. (a) laminar flow; and (b) turbulent flow. Part (c) gives the calculated Ca^{2+} concentrations at saturation, $[Ca^{2+}]_{eq}$ in 10^{-4} mmol cm^{-3}

δ (cm)	$P_{CO_2} = 1 \cdot 10^{-2}$ atm.			$P_{CO_2} = 3 \cdot 10^{-2}$ atm.			$P_{CO_2} = 5 \cdot 10^{-2}$ atm.			$P_{CO_2} = 1 \cdot 10^{-1}$ atm.		
	5°C	10°C	20°C	5°C	10°C	20°C	5°C	10°C	20°C	5°C	10°C	20°C
(a) *Laminar flow:*												
0.001	0.714	1.6	7.14	0.606	1.1	3.33	0.666	1.19	3.33	0.833	1.39	3.23
0.002	1.3	2.8	13.3	1.18	2.1	6.25	1.25	2.25	5.26	1.05	1.73	3.33
0.005	3.13	6.4	21.7	2.13	3.5	8.93	1.49	2.5	5.0	1.06	1.73	3.33
0.01	5.26	9.6	21.7	2.04	3.5	8.7	1.49	2.47	4.76	1.06	1.73	3.23
0.02	5.13	9.5	18.2	2.0	3.46	6.9	1.46	2.44	4.76	1.05	1.70	3.17
0.05	4.76	8.4	16.1	2.0	3.3	6.5	1.43	2.43	4.67	1.04	1.68	3.07
0.1	4.08	7.7	12.7	1.89	3.25	5.9	1.4	2.29	4.46	1.01	1.61	2.95
(b) *Turbulent flow:*												
0.001	1.08	3.3	9.75	0.63	1.08	4.1	0.655	1.17	3.37	0.82	1.37	3.5
0.003	2.9	7.3	22.0	1.8	3.3	9.5	1.97	3.32	8.14	2.28	3.5	6.0
0.005	5.08	10.2	27.5	2.9	5.1	13.0	3.13	5.09	10.4	3.3	4.7	7.8
0.01	8.6	15.1	34.0	5.4	8.75	17.0	5.2	7.3	13.0	4.54	6.05	9.0
0.02	13.2	20.5	45.0	8.2	11.3	19.0	6.9	8.9	13.9	5.5	7.0	10.2
(c) *Ca^{2+} concentrations at saturation:*												
$[Ca^{2+}]_{eq}$	6.4	5.5	4.1	16.6	14.4	11.0	24.3	21.4	16.9	38.8	35.1	28.0

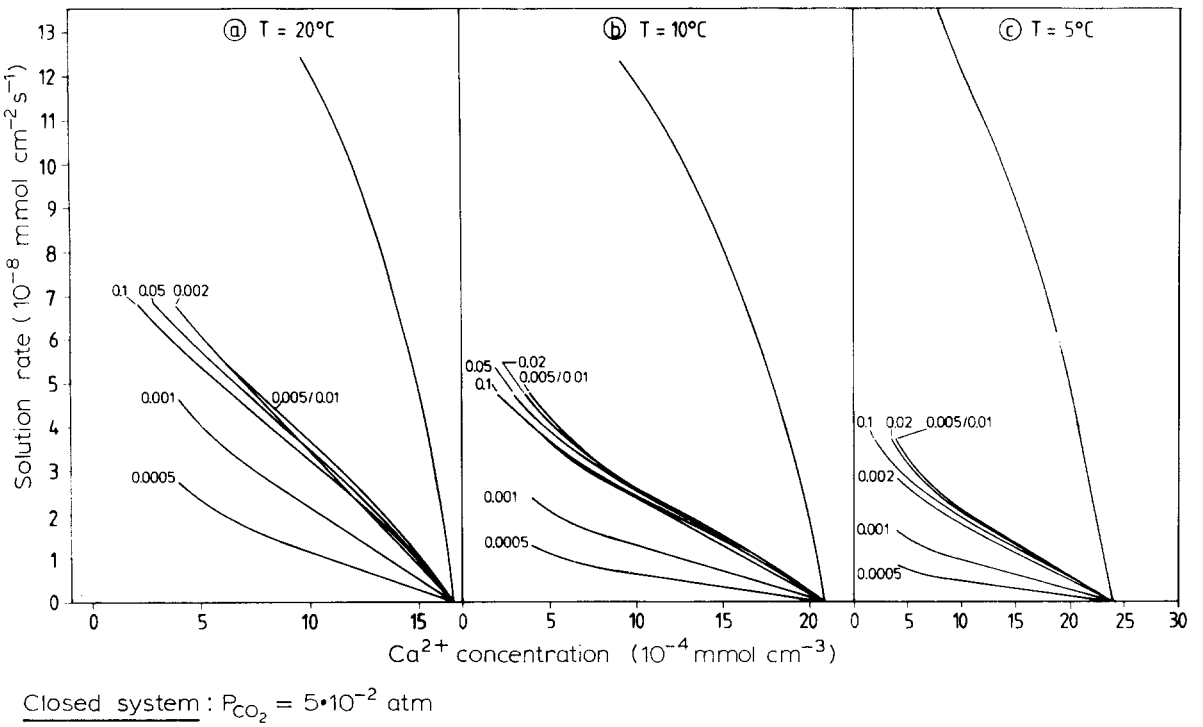

Fig. 3. Calculated dissolution rates at $P_{CO_2} = 5 \cdot 10^{-2}$ atm. for various film thicknesses and temperatures as function of the average Ca^{2+} concentration. The *number on the solid lines* gives the film thickness δ in cm. The upmost curves represent turbulent flow conditions and are calculated for $\delta = 1$ cm.

rate limiting. We have found the same behaviour in the open system (Buhmann and Dreybrodt, 1985), and have there in detail discussed its physical reasons. The temperature dependence of α is determined by the temperature dependence of the CO_2 conversion and therefore α decreases with decreasing temperature.

At $\delta \geqslant 0.01$ cm a threshold is reached (cf. Fig. 3) and the rates decrease with increasing film thickness. In the threshold region the rates are determined by chemically enhanced diffusion of CO_2 and above the threshold diffuson of Ca^{2+} becomes rate limiting. For values of $[Ca^{2+}]_{av} \leqslant 0.2[Ca^{2+}]_{eq}$ a steep increase in the rate curves appears. We will not treat this effect further, since most of the dissolution proceeds in the region of higher $[Ca^{2+}]_{av}$ and our experiments give data in this region.

For all cases where diffusion and CO_2 conversion determine the dissolution process, a change of the surface kinetics only slightly changes the dissolution rates. We have changed the reaction constants (κ_i) in the PWP equation (1) by factors of 2 and of 0.5 and found a change in dissolution rates in both cases of only $\sim 20\%$. Thus, during dissolution processes at karst initiation, where laminar flow at small δ prevails, all effects which change the surface kinetics, e.g. lithology, should be of minor influence.

In contrast to the lower curves which simulate the case of laminar flow, where D and D_{CO_2} are the molecular coefficients of diffusion, the upmost curves in Fig. 3 simulate turbulent flow. In this case eddy diffusivities D_e are used, which are higher by a factor of 10^4. In this case neither CO_2 conversion nor diffusion are rate limiting and the process is entirely controlled by surface kinetics as given by the PWP equation (1). If in turbulent flow δ is small, then CO_2 conversion again is important in determining the rates. We will discuss this on the next page.

For the moment, we state the fact that at

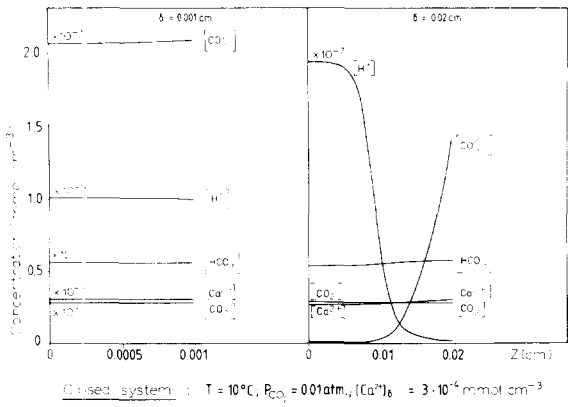

Fig. 4. Concentration profiles of the five most important species across water films of 0.001 and 0.02 cm thickness, respectively. The concentration scale for the individual species has to be multiplied by the *factor* given *on the* corresponding *curve*.

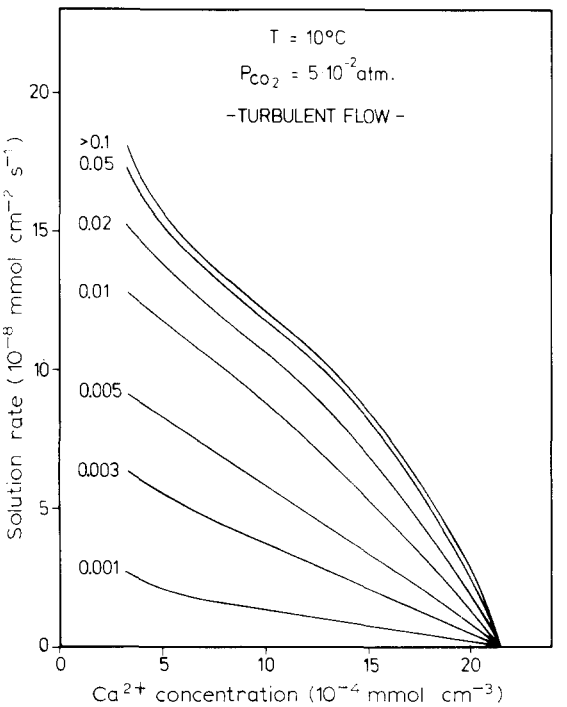

Fig. 5. Calculated dissolution rates under turbulent-flow conditions for various film thicknesses δ. The *number on the solid lines* gives δ in cm. The upmost curve indicates the limit of infinite film thickness.

sufficiently high δ the dissolution rates, once turbulent flow sets in, are increased by one order of magnitude compared to laminar flow. This hydraulic jump, which we have found as well under open-system conditions, is of utmost importance in the development of cave systems.

To demonstrate the region of CO_2 conversion and of chemically enhanced diffusion (threshold) we have calculated the concentration profiles for the case of $P^i_{CO_2} = 10^{-2}$ atm. and $[Ca^{2+}]_\delta = 3 \cdot 10^{-4}$ mmol cm^{-3} at 10°C for two film thicknesses. Fig. 4 gives the results. At $\delta = 0.001$ cm the distance is so small that effects of diffusion can be neglected. In this case almost no concentration gradients build up. At higher values of $\delta \geqslant 0.02$ cm strong concentration gradients build up and there is a flow of H^+ towards the solid interface and a flow of CO_3^{2-} directed away from it. In the region of ~ 0.01 cm thickness in front of the $CaCO_3$ solid CO_3^{2-} combines with H^+, and HCO_3^- is produced. The thickness of this region is determined by production of H^+ via $CO_2 \rightarrow H^+ + HCO_3^-$ conversion and by diffusion, and it thus depends on the conversion constants and D.

We now come back to the discussion of dissolution under turbulent flow. Fig. 5 shows dissolution rates with an eddy diffusivity $D_e = 10^4 D_{CO_2}$ for various film thicknesses δ at $P^i_{CO_2} = 5 \cdot 10^{-2}$ atm. and $T = 10$°C. Since diffusion is no more of importance, we find that no threshold is reached, behind which the rates decrease with increasing film thickness. At low $\delta \leqslant 0.005$ cm the rates increase linearly with δ, since in this region CO_2 conversion is rate limiting.

For $\delta > 0.005$ cm, CO_2 conversion and surface kinetics both determine the dissolution rates and the rates increase much slower with δ until a threshold is reached at $\delta \geqslant 0.1$ cm, where surface kinetics control the dissolution entirely. This is the case for all $P^i_{CO_2}$ with 0.01 atm. $\leqslant P^i_{CO_2} \leqslant$ 0.1 atm. In Fig. 6 we have therefore given the dissolution rates for $\delta \geqslant 0.1$ cm for various $P^i_{CO_2}$ pressures at 10°C. Since we expect that in real karst systems turbulent flow sets in at δ in the order of a few millimeters these curves describe realistic dissolution rates. We have

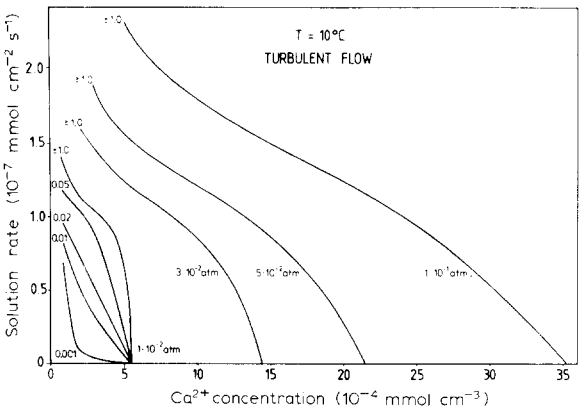

Fig. 6. Calculated dissolution rates under turbulent flow conditions for various CO_2 pressures and various film thicknesses δ in the case of $P_{CO_2} = 10^{-2}$ atm. The *number on the solid lines* gives δ in cm.

calculated the same dissolution rates in a previous work (Dreybrodt, 1981a, fig. 1), by assuming equilibrium between all species and neglecting effects of diffusion and CO_2 conversion.

One important fact should be stated. At low $P^i_{CO_2}$ pressures ($\leqslant 0.05$ atm.) and $\delta \geqslant 0.05$ cm the linear relation of eq. 21 no longer holds. The rates can then be approximated by two linear regions, one with lower slope at lower $[Ca^{2+}]_{av}$ and the other with higher slope at higher $[Ca^{2+}]_{av}$. In Table II we have listed the values of α for these cases together with the corresponding equilibrium values of Ca^{2+}, $[Ca^{2+}]_{eq}$ and $[Ca^{2+}]_{as}$.

$[Ca^{2+}]_{as}$ is the intersection point of the straight line representing the region of lower slope with the Ca^{2+}-axis. These values of Table II are the relevant ones for turbulent-flow conditions, since turbulence is only possible in sufficiently thick water films, i.e. $\delta > 0.1$ cm (Dreybrodt, 1981b). Nevertheless we have listed the values of α for $\delta \leqslant 0.02$ cm in Table I for completeness. In this region the normal linear relationship:

$$R = \alpha([Ca^{2+}]_{eq} - [Ca^{2+}]_{av})$$

holds reasonably well for all values of $[Ca^{2+}]_{av}$.

In all our calculations we have assumed $D_e = nD$, $n = 10^4$. It is important, however, to know the dependence of the dissolution rates on the values of n. We therefore have

TABLE II

Calculated values of α for various pressures of CO_2 and temperatures at turbulent flow and film thicknesses > 0.02 cm

δ (cm)	$P_{CO_2} = 1\cdot10^{-2}$ atm.			$P_{CO_2} = 3\cdot10^{-2}$ atm.			$P_{CO_2} = 5\cdot10^{-2}$ atm.			$P_{CO_2} = 1\cdot10^{-1}$ atm.		
	5°C	10°C	20°C	5°C	10°C	20°C	5°C	10°C	20°C	5°C	10°C	20°C
(a) $[Ca^{2+}]_{av} > 0.7[Ca^{2+}]_{eq}$:												
0.05	2.4	4.2	11.8	1.4	2.1	2.6	1.0	1.4	2.3	0.76	0.93	1.8
0.1	4.0	6.7	17.3	1.7	2.5	2.8	1.2	1.5	2.4	0.8	1.0	1.8
0.3	9.8	14.3	29.2	1.8	2.5	2.8	1.3	1.5	2.4	0.8	1.0	1.8
$[Ca^{2+}]_{eq}$	6.4	5.5	4.1	16.6	14.4	11.0	24.3	21.4	16.9	38.8	35.1	28.0
(b) $[Ca^{2+}]_{av} < 0.7[Ca^{2+}]_{eq}$:												
0.05	1.5*	1.3*	1.6	0.6	0.78	1.3	0.54	0.67	1.0	0.44	0.56	0.7
0.1	0.85	1.0	1.7	0.63	0.82	1.35	0.56	0.69	1.02	0.45	0.57	0.7
0.3	0.9	1.0	1.7	0.65	0.82	1.35	0.56	0.69	1.02	0.45	0.57	0.7
$[Ca^{2+}]_{as}$	8.0*	9.7*										
	14.2	13.3	9.3	24.0	20.5	16.0	31.0	27.5	22.0	47.5	41.5	34.0

Values of α in 10^{-4} cm s^{-1}; $[Ca^{2+}]_{eq}$ and $[Ca^{2+}]_{as}$ in 10^{-4} mmol cm^{-3}. $[Ca^{2+}]_{as}$ is an apparent saturation concentration of Ca^{2+} as discussed in the text.
*Corresponding values for $T = 5$°C and $T = 10$°C in this special case.

calculated dissolution rates for the case of $T = 20°C$, $P^{i}_{CO_2} = 5 \cdot 10^{-2}$ atm. and $[Ca^{2+}]_\delta = 10^{-3}$ mmol cm^{-3} for various δ and n. Fig. 7 shows the results. At low water film thickness, $\delta = 0.001$ cm, diffusional processes play no important role even at $n = 1$. In this case no dependence on n is observed and laminar or turbulent flow give the same results in dissolution. As δ increases a dependence on n develops. Diffusional processes can thus be neglected at $\delta = 0.01$ cm for values of $n \geqslant 10^3$ and at $\delta > 0.1$ cm for $n \geqslant 10^4$.

These calculations are important for calculations of dissolution processes in porous media, where turbulence sets in at much lower Reynolds numbers ($N_{Re} = 10$—100) than in conduits ($N_{Re} \approx 2000$), and where diffusivity is also controlled by mechanical dispersion (Bear, 1972). Our theory can be applied to calculate dissolution rates in porous media. Here δ is to be replaced by an effective diameter of the flow channels (Baumann et al., 1985).

As we have already stated, our theory can be used also to calculate precipitation rates under closed-system conditions. Precipitation occurs when calcareous solutions enter a cave and equilibrate with the CO_2 pressure of the cave. This produces a supersaturated solution, which eventually enters joints. This solution will then deposit $CaCO_3$ and accordingly release CO_2 into the water film. Thus, deposition takes place until the dissolved $CaCO_3$ and the CO_2 concentration are in equilibrium. This mechanism might be responsible for

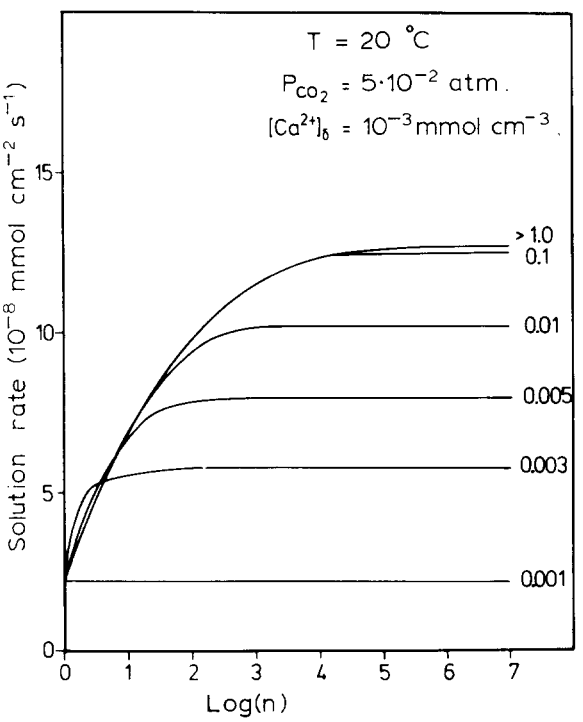

Fig. 7. Calculated dissolution rates for various film thicknesses δ as a function of the factor n. The diffusion coefficient D_{CO_2} is multiplied by the factor n to give the effective diffusion coefficient D_e for the calculations. The *number on the curves* gives δ in cm.

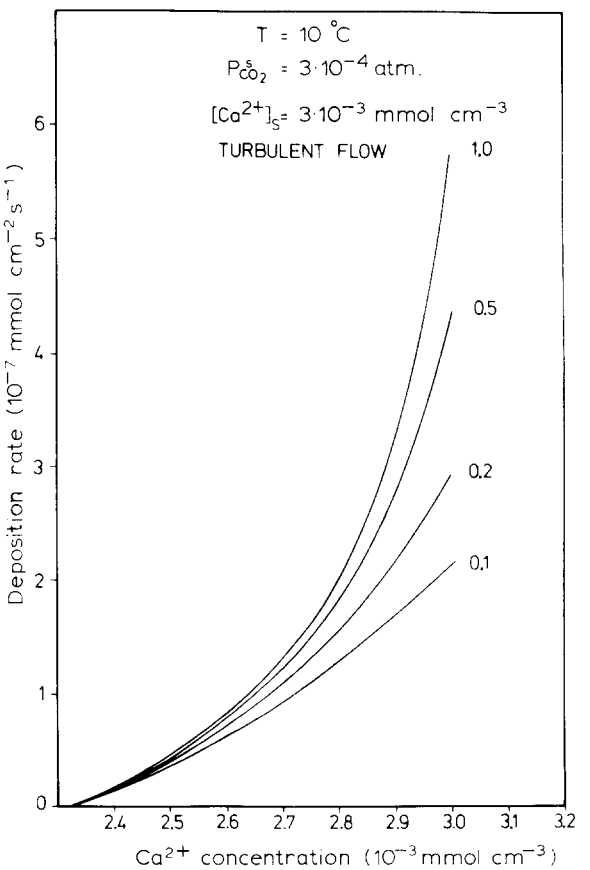

Fig. 8. Calculated deposition rates under turbulent-flow conditions at various film thicknesses δ. The solution enters the closed system with $P_{CO_2} = 3 \cdot 10^{-4}$ atm. and a Ca^{2+} concentration of $3 \cdot 10^{-3}$ mmol cm^{-3}. The *number on the curves* gives δ in cm.

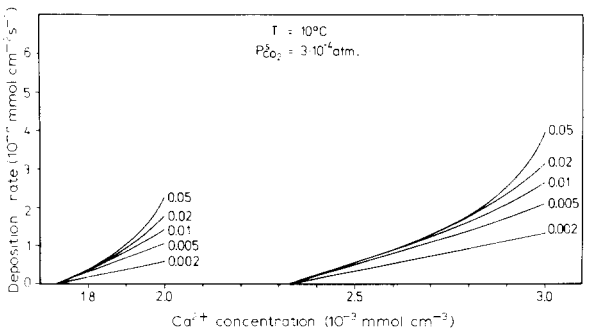

Fig. 9. Calculated deposition rates at various film thicknesses δ and two different initial Ca^{2+} concentrations of $2 \cdot 10^{-3}$ and $3 \cdot 10^{-3}$ mmol cm^{-3}, respectively. The *number on the curves* gives δ in cm. The solution enters the closed system with $P_{CO_2} = 3 \cdot 10^{-4}$ atm.

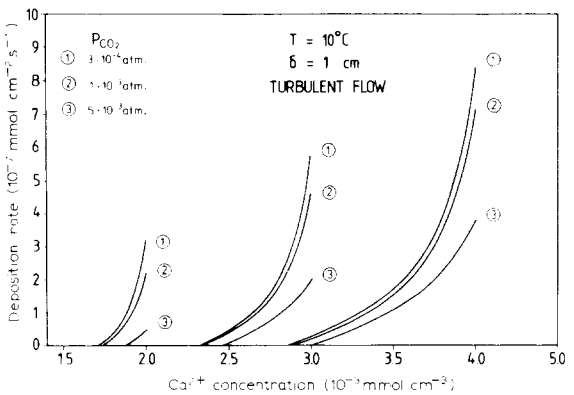

Fig. 10. Calculated deposition rates under turbulent-flow conditions at various initial CO_2 pressures and initial Ca^{2+} concentrations.

closing of sufficiently narrow joints and for changing the subterranean percolation route.

Fig. 8 shows a representative example. Water with $[Ca^{2+}]_s = 3 \cdot 10^{-3}$ mmol cm^{-3} has equilibrated with an atmosphere containing CO_2 with a partial pressure of $3 \cdot 10^{-4}$ atm. On entering joints of width 2δ precipitation takes place under turbulent flow conditions.

Fig. 9 shows the same situation for the case of laminar flow for two values of initial $[Ca^{2+}]_s$. In laminar flow precipitation rates are lower by a factor of ~ 10. This again illustrates the hydraulic jump. To estimate the time required to close a joint under constant rates of precipitation, we note that a deposition rate of 10^{-7} mmol cm^{-2} s^{-1} causes a deposition of 0.1174 cm $yr.^{-1}$ on each wall of the joint (Dreybrodt, 1980). Thus, closing of joints can proceed in a very short time.

Fig. 10 shows precipitation rates for $\delta = 1$ cm at various $P^i_{CO_2}$ pressures and various values of $[Ca^{2+}]_s$ of the solution entering the joint under turbulent flow, to give some illustrations about the variations of precipitation rates which can be expected.

3. Experimental

3.1. Experimental method

To prove our theoretical results we used a procedure similar to that in our work on open systems (Buhmann and Dreybrodt, 1985). We measured the time dependence of $[Ca^{2+}]_{av}$ during dissolution in a stagnant H_2O film enclosed by two parallel calcite surfaces with distance 2δ. As long as the dissolution rates are given by a linear relation according to eq. 21 the time dependence of the average Ca^{2+} concentration is:

$$[Ca^{2+}]_{eq} - [Ca^{2+}]_{av}(t) = [Ca^{2+}]_{eq} \exp(-t/\tau) \qquad (22)$$

with

$$\tau = \delta/\alpha$$

Thus, from the exponential decay of the quantity $\{[Ca^{2+}]_{eq} - [Ca^{2+}]_{av}(t)\}$ towards zero the time constant τ can be measured and be compared to the theoretical value of τ. In Section 2.1 we have stated that the time development of $[Ca^{2+}]_{av}(t)$ in a stagnant film is equal to that of laminar or turbulent plug flow and thus our experiment simulates well the natural situation.

The calcite specimens are flat plates with dimensions 5 cm × 10 cm × 1 cm, cut from white marble (Carrara). They were surface polished and etched with dilute HCl and washed carefully with distilled water before first use. To simulate the conditions of laminar flow two of these plates were mounted with a distance $d = 2\delta$ towards each other. The distance was achieved by placing

distance pieces of Teflon® at the rims. Then the volume between the plates was filled with double-distilled water of known CO_2 content and the system was closed with respect to the surroundings to prevent CO_2 exchange. After a time t the solution was extracted with a syringe which was mounted into one of the calcite plates. The solution was then analyzed for its Ca^{2+} concentration by atomic absorption spectroscopy.

All the experiments were performed in a temperature-regulated thermostatic chamber ($T \pm 0.5°C$). The solutions with fixed CO_2 content were prepared by bubbling an artificial commercially available atmosphere with known CO_2 content through double-distilled water and monitoring pH to control equilibrium.

To simulate the conditions of turbulent flow, a calcite specimen of 6 cm diameter and 1 cm thickness was mounted from below, by using O-ring seals of Teflon®, to a cylindrical Teflon® beaker with inner diameter of 3.8 cm and of known inner height δ. Through the upper side a glass stirrer was introduced, which was tightened by a Simmering® seal. The CO_2-containing solution was introduced through one inlet until the solution flows out at a comparable outlet. Thus, one could ascertain that no air bubbles remained in the chamber. The inlet and the outlet were then sealed against the outer atmosphere. By stirring the solution the effective diffusion coefficient was enhanced by a factor of 10^3 (cf. Buhmann and Dreybrodt, 1985). The thicknesses of the solution in these experiments were 1, 1.5 and 2 cm. The solution was extracted from the container after a time t and analyzed for $[Ca^{2+}]$.

3.2. *Experimental results*

Fig. 11a shows the time constants measured from the exponential behaviour of $[Ca^{2+}](t)$ for laminar flow simulation at $P^i_{CO_2} = 10^{-2}$ atm. for 10° and 20°C. The full lines represent the theoretically predicted increase of τ vs. δ.

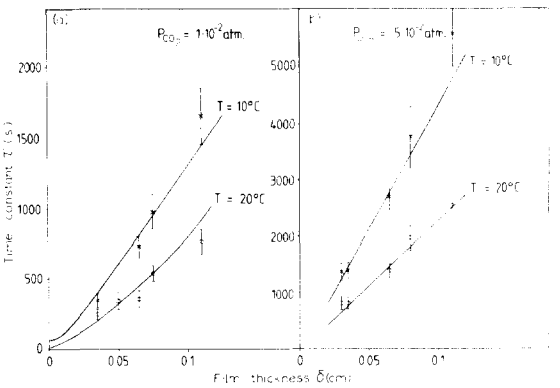

Fig. 11. Time constants of $CaCO_3$ dissolution measured for various film thicknesses, temperatures and CO_2 pressures. The *solid lines* are the theoretical curves; the measurements were performed on pure Carrara marble.

The agreement with the experimentally observed values is excellent. In Fig. 11b experimental and theoretical data are given for solutions with $P^i_{CO_2} = 5 \cdot 10^{-2}$ atm. at 10° and 20°C. Again theory and experiment show similar good agreement. One should note that at lower initial CO_2 pressures the time constants are significantly lower. That means that, as in the case of the open system, equilibrium is achieved faster than at high CO_2 content. The dissolution rates, however, are higher at higher CO_2 content, because more CO_2 can be converted into HCO_3^- and H^+.

For the case of turbulent flow an increase in dissolution rates by one order of magnitude was predicted. We have simulated these conditions by stirring solutions with ~ 200 r.p.m. This leads to an increase of $D_e \approx 10^3 D_{CO_2}$. From Fig. 7 one sees that at this value of n the dissolution rate is ~ 90% of that of fully developed turbulence. This is sufficient for our purpose. Fig. 12 shows the results for initial pressures of 10^{-2} and $5 \cdot 10^{-2}$ atm. at temperatures of 20°C. The full lines represent the theoretically predicted time constants multiplied by a fitting factor of 1.7. A similar fitting factor, indicating that in nature dissolution proceeds slower, has also been observed in our turbulence experiments under open-system conditions. Since under turbulent flow only the

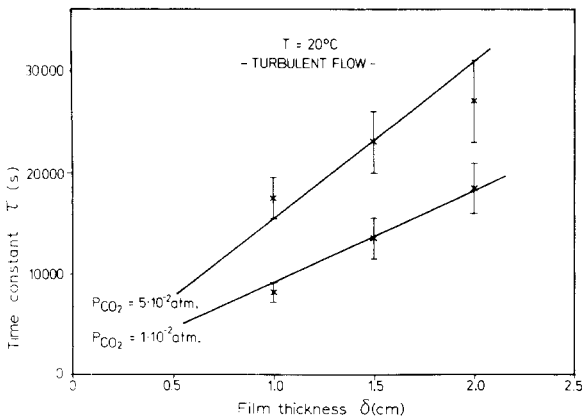

Fig. 12. Time constants of $CaCO_3$ dissolution under turbulent-flow conditions measured at various film thicknesses and CO_2 pressures, respectively. The *solid lines* give the theoretical curves fitted to the experimental results by a factor as discussed in the text. The measurements were performed on pure Carrara marble.

surface kinetics determine the dissolution rates, we may conclude that in marble, which contains ~ 2 wt.% Mg, dissolution is lower than in pure calcite. This would mean that the rate constants in the PWP equation are reduced in this natural limestone. This might happen by Langmuir adsorption of Mg^{2+}, which reduces the effective surface active in the dissolution processes (Sjöberg, 1978). Nevertheless, our theoretical predictions are sufficiently accurate for geological applications.

A second point should be mentioned, which is important in this type of experiment. As discussed in relation to Table II (Section 2.3) we have to approximate the calculated dissolution rates at $\delta > 0.2$ cm by two different linear functions. In the region of the experimentally occurring Ca^{2+} concentrations we have to take α from the region of lower slope [Table II, (b)], which gives an apparently higher Ca^{2+} concentration in equilibrium, $[Ca^{2+}]_{as}$. The data in Fig. 12 have been obtained from these values.

Summarizing our experimental results, we can state that agreement between experiment and theory is good in the case of closed-system conditions. Since we have obtained a similar good agreement in the case of dissolution and precipitation experiments in the open system, we can be quite sure that our theory is well applicable to all cases of interest and we can trust the predictions of precipitation rates under closed-system conditions. Experiments for this case have not yet been performed since they are far more difficult.

4. Conclusion

Our theory of calcite dissolution and precipitation has been applied to closed-system conditions and provides in addition to our previous results on open systems a comprehensive kinetic theory on pure $CaCO_3$–CO_2–H_2O systems. All experiments show convincing coincidence with the overall behaviour of the theoretical predictions. Thus we conclude that the theory is applicable with sufficient reliability to many geological problems in karst areas. One important result is the verification of the hydraulic jump, i.e. the increase of dissolution and precipitation rates by one order of magnitude at the onset of turbulent flow. This is of utmost importance in the development of water conduits during the process of karstification.

Our theory for the closed system can also be extended to the more complicated situation of porous saturated media consisting of $CaCO_3$. If one assumes that dissolution in such media can be described by using the average channel width in those media as the distance 2δ in our simple geometry model and if one replaces the coefficient of diffusion by the coefficient of mechanical dispersion one obtains predictions in excellent agreement with experimental data (Baumann et al., 1985).

Our results given in Tables I and II can be used by the geologist to estimate dissolution rates in many situations and should therefore provide deeper insight into the dynamics of karstification. In the future we will extend our work to natural systems. Experiments in the turbulent flow regime are in progress

to investigate the effects of the chemical composition and lithology of limestones on the surface kinetics. Experiments with natural waters containing SO_4^{2-}, Cl^-, Mg^{2+}, Na^+ and K^+ can give insight into changes of the dissolution rates by altering the chemical composition of the solvent compared to pure H_2O—CO_2 solvents.

Acknowledgements

The authors thank Mr. G. Ankele for his technical assistance in planning and setting up of the experiments. The project was financially supported by the Deutsche Forschungsgemeinschaft (Schwerpunktprogramm: Hydrogeochemische Vorgänge im Wasserkreislauf der ungesättigten und gesättigten Zone).

References

Baumann, J., Buhmann, D., Dreybrodt, W. and Schulz, H.D., 1985. Calcite dissolution kinetics in porous media. Chem. Geol., 53: 219—228 (this volume).

Bear, J., 1972. Dynamics of Fluids in Porous Media. American Elsevier, New York, N.Y., 764 pp.

Buhmann, D. and Dreybrodt, W., 1985. The kinetics of calcite dissolution and precipitation in geologically relevant situations of karst areas, 1. Open system. Chem. Geol., 48: 189—211.

Carslaw, H.S. and Jaeger, J.C., 1959. Conduction of Heat in Solids. Oxford at the Clarendon Press, London, 2nd ed., 510 pp.

Dreybrodt, W., 1980. Deposition of calcite from thin films of natural calcareous solutions and the growth of speleothems. Chem. Geol., 29: 89—105.

Dreybrodt, W., 1981a. Kinetics of the dissolution of calcite and its application to karstification. Chem. Geol., 31: 245—269.

Dreybrodt, W., 1981b. Mixing corrosion in $CaCO_3$—CO_2—H_2O systems and its role in the karstification of limestone areas. Chem. Geol., 32: 221—236.

Howard, A.D. and Howard, B.Y., 1967. Solution of limestone under laminar flow between parallel boundaries. Caves Karst, 9: 25—40.

Kamke, E., 1967. Differentialgleichungen. Akademische Verlagsgesellschaft. Geest & Portig, Leipzig, 664 pp.

Kern, M.D., 1960. The hydration of carbon dioxide. J. Chem. Educ., 37: 14—23.

Plummer, L.N., Wigley, T.M.L. and Parkhurst, D.L., 1978. The kinetics of calcite dissolution in CO_2—water systems at 5°C to 60°C and 0.0 to 1.0 atm. CO_2. Am. J. Sci., 278: 179—216.

Plummer, L.N., Parkhurst, D.L. and Wigley, T.M.L., 1979. Critical review of the kinetics of calcite dissolution and precipitation. In: E.A. Jenne (Editor), Chemical Modeling in Aqueous Systems. Am. Chem. Soc., Symp. Ser., 93: 537—573.

Quinn, J.A. and Otto, N.C., 1971. Carbon dioxide exchange of the air—sea interface: flux augmentation by chemical reaction. J. Geophys. Res., 76: 1539—1549.

Rauch, H.W. and White, W.B., 1977. Dissolution kinetics of carbonate rocks, 1. Effects of lithology on dissolution rate. Water Resour. Res., 13: 381—394.

Sjöberg, E.L., 1978. Kinetics and mechanism of calcite dissolution in aqueous solutions at low temperatures. Stockholm Contrib. Geol., 32: 1—92.

Skelland, A.H.P., 1974. Diffusional Mass Transport. Wiley, New York, N.Y., 510 pp.

Usdowski, E., 1982. Reactions and equilibria in the systems CO_2—H_2O and $CaCO_3$—CO_2—H_2O (0°—50°C) — A review. Neues Jahrb. Mineral. Abh., 144: 148—171.